1998

Electrochemical Investigations of Cobalt-Doped $LiMn_2O_4$ as Cathode Material for Lithium-Ion Batteries

P. Arora
University of South Carolina - Columbia

Branko Popov
University of South Carolina - Columbia, popov@engr.sc.edu

Ralph E. White
University of South Carolina - Columbia, white@cec.sc.edu

Publication Info

Journal of the Electrochemical Society, 1998, pages 807-815.

Publisher's link: http://dx.doi.org/10.1149/1.1838349
DOI: 10.1149/1.1838349

Electrochemical Investigations of Cobalt-Doped $LiMn_2O_4$ as Cathode Material for Lithium-Ion Batteries

P. Arora,* B. N. Popov, and R. E. White****

Center for Electrochemical Engineering, Department of Chemical Engineering, University of South Carolina, Columbia, South Carolina 29208, USA

ABSTRACT

A wide range (y = 0.05–0.33) of Co-doped $LiCo_yMn_{2-y}O_4$ spinels were synthesized and electrochemically characterized. These Co-doped spinels showed improved specific capacity and capacity retention over pure spinels. Electrochemical impedance spectroscopy and the linear polarization resistance technique were used to determine the transport and electrochemical kinetic parameters of Co-doped spinels. The presence of Co in the spinel inhibits the passivation process occurring on the surface of the cathode. Also, Co increases the exchange current density and facilitates the charge-transfer reaction of the active material. The lower self-discharge observed for Co-doped spinels was attributed to their low surface areas. The cumulative capacity loss estimated for a pure spinel resulting from self-discharge in the first 30 h was 3 and 6 times larger than those estimated for Co-doped spinels with y = 0.05 and y = 0.16 in $LiCo_yMn_{2-y}O_4$, respectively.

Introduction

Layered $LiCoO_2$ is currently used as a cathode material for production of commercial, high-energy-density lithium-ion batteries.[1,2] Because of the high cost of Co and its toxicity, the three-dimensional $LiMn_2O_4$ spinel phase was studied extensively to substitute $LiCoO_2$ as the cathode material for Li-ion batteries.[3-8] The Li insertion–deinsertion processes occur in the spinel phase in two composition ranges resulting in two voltage plateaus at 4 and 3 V vs the Li/Li^+ reference electrode.[9,10] Attempts to substitute $LiMn_2O_4$ for $LiCoO_2$ in commercial Li-ion batteries have not been successful due to the lower specific capacity of the spinel and the fast capacity fade upon cycling.[11-13]

Efforts have been made to improve cycle life by controlling the capacity fading in $LiMn_2O_4$.[3,5,10-17] The capacity fading has been attributed to spinel dissolution,[11] the Jahn–Teller effect,[12] and lattice instability[13] at high oxidation levels. Baochen et al.[15] found that cobalt-doped $LiCo_yMn_{2-y}O_4$ improved cycling performance. According to Guohua et al.,[12] $LiCo_{1/6}Mn_{11/6}O_4$ showed good cycle performance with an energy density of 370 Wh/kg at the 300th cycle. Recently, Sanchez and Tirado[16] reported a new cobalt-substituted Li_2O-$y$$MnO_2$ (y = 4) spinel phase reversible in a 3.3–2.3 V potential window. The capacity for the first cycle was 165 mAh/g. However, the initial capacity decreased sharply during the first five cycles, reaching values of about 110 and 85 mAh/g after 100 and 200 cycles, respectively.

In this study, a wide range (y = 0.05–0.33) of Co-doped $LiCo_yMn_{2-y}O_4$ spinels was synthesized and electrochemically characterized. Electrochemical impedance spectroscopy (EIS) and the linear polarization resistance technique (LP) were used to determine the transport and electrochemical kinetic parameters of pure and Co-doped spinels.

The capacity fade rates of $LiMn_2O_4$ and $LiCo_yMn_{2-y}O_4$ were studied and the active material loss during cycling was determined. Also, the effect of Co content on the self-discharge of pure and Co-doped $LiMn_2O_4$ was investigated.

Experimental

$LiMn_2O_4$ and Co-doped $LiMn_2O_4$ cathodes were prepared by a solid-state reaction between lithium carbonate (Aldrich, 99%), manganese carbonate (Aldrich, 99.9%), and cobalt oxalate hydrate (Aldrich, 99%). The mixture was preheated at 600 °C for 6 h and then heated at 750 °C for 3 days in air with intermittent grinding, followed by slow cooling (about 2 °C/min) to cool the sample to ambient temperature. $LiCo_yMn_{2-y}O_4$ compounds with y = 0, 0.05, 0.06, 0.08, 0.16, and 0.33 were prepared.

The active material was mixed with carbon black and Teflon binder in a ratio of $LiCo_yMn_{2-y}O_4$:carbon black:Teflon = 100:10:5 by weight and pressed into a thin film. Scanning electron microscopy (SEM) and X-ray diffraction (XRD) studies were carried out to determine the particle size and the structure of the synthesized cathode materials. Electrochemical characterization of the cathode materials was carried out using Swagelok three-electrode cells presented in Fig. 1. The anode and reference electrodes were disks of lithium foil, and a sheet of glass fiber acted as the separator. The electrolyte contained 1 M $LiPF_6$ dissolved in a mixture of propylene carbonate (PC), ethylene carbonate (EC), and dimethyl carbonate (DMC) in a ratio 1:1:3. The T-cell was assembled in a glove box filled with argon. The cathode had a diameter of 1.25 cm (an area of 1.23 cm^2) and a thickness of 70 μm with a total mass of 20 mg. It was heated in a minifurnace at 300 °C for 2 h in the glove box before assembling. The cathode and anode separation was approximately 3 mm. After the cell was assembled, it was left in the dry box for half an hour, enabling the electrolyte to disperse into the porous structure of the cathode. The cells were tested with a Bitrode (Bitrode Co., MI, USA) cycler with cutoff potentials of 3 and 4.3 V. Charge/discharge curves were obtained galvanostatically using a current density of 0.1 mA/cm^2.

Cyclic voltammograms were obtained using a scan rate of 0.06 mV/s over a potential range of 3.0 to 4.3 V vs Li/Li^+ reference electrode. EIS experiments were carried out at different states of charge on both pure spinel and Co-doped spinel electrodes with y = 0.160 in $Li_xCo_yMn_{2-y}O_4$. The impedance data generally covered the frequency range from 0.002 Hz to 100 kHz with an ac voltage signal of ±5 mV, which ensured the electrode system to be under minimum perturbation. The Co-doped spinels were characterized by XRD using a Rigaku 405S5 diffractometer with

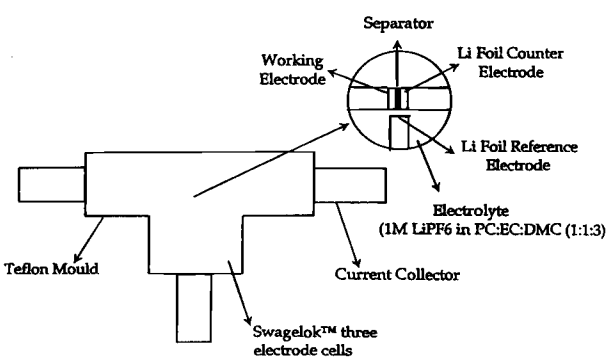

Fig. 1. Schematic of a T-cell.

* Electrochemical Society Student Member.
** Electrochemical Society Active Member.

Cu K_α radiation. The specific surface area was measured using a Micrometrics Pulse Chemisorb 2700 according to the Brunauer-Emmett-Teller (BET) single-point method with nitrogen physiosorption. All samples were previously dried for half an hour under argon flow at 150 °C.

Results and Discussion

The powder XRD patterns of the $LiCo_yMn_{2-y}O_4$, for y = 0, 0.08, 0.160, and 0.330 are shown in Fig. 2. All samples were identified as a single-phase spinel with a space group Fd3m (oh^7) where lithium ions occupy the tetrahedral (8a) sites; Mn^{3+}, Mn^{4+}, and Co^{3+} ions reside at the octahedral 16(d) sites; and O^{2-} ions are located at 32(e) sites. The estimated structure agreed with previous results obtained for pure spinel.[14,15]

The lattice constants of $Li_xCo_yMn_{2-y}O_4$ ($0 < y < 1$) samples are presented in Fig. 3 as a function of the Co content in the oxide. The cubic lattice parameter "a" was estimated for the fully discharged electrode. Fully discharged spinel (x = 1 and y = 0) has a lattice constant value of 8.24 Å. Guohua et al.[12] studied the cubic lattice constant "a" variation as a function of x for $Li_xM_{1/6}Mn_{11/6}O_4$ (M = Cr, Ni, or Co). They found that a-values decreased with the deintercalation of lithium in the positive electrode. The variation of the lattice parameter was almost linear with an a-value of 8.042 Å for a charged electrode ($Li_{0.11}Mn_2O_4$). As shown in Table I, in the Co-substituted spinel phases, the Mn–Mn and Mn–O interatomic distances decreased with increasing Co content thereby contributing to the spinel lattice contraction and to the decrease of the initial specific capacity of the doped spinel. The average Mn–Mn and Mn–O interatomic distances were calculated using the equation $R_{Mn-Mn} = a\sqrt{2}/4$ and $R_{Mn-O} = a(3u^2 - 2u + 0.375)^{0.5}$, respectively. The constant u = 0.265 is the oxygen positional parameter,[8] considered constant for all samples. As shown in Fig. 3, the lattice constant decreased linearly with increasing Co content. For example when y = 1 in $Li_xCo_yMn_{2-y}O_4$, the spinel lattice constant decreased to 8.09 Å.

Table I. Lattice constants, unit cell volume, and interatomic distances for $LiCo_yMn_{2-y}O_4$ samples.

y	a (Å)	V (Å^3)	R_{Mn-Mn}	R_{Mn-O}
0.00	8.249	561.31	2.916	1.946
0.08	8.229	557.24	2.919	1.942
0.17	8.205	552.38	2.900	1.936
0.33	8.169	545.14	2.888	1.927
0.50	8.137	538.76	2.876	1.919
0.67	8.139	539.15	2.877	1.920
0.83	8.114	534.20	2.868	1.914
1.00	8.097	530.85	2.863	1.910

The $Li/Li_xCo_yMn_{2-y}O_4$ volume change during the cycling for y = 0 (V = 559.68 Å^3 for a fully intercalated spinel and V = 520.69 Å^3 for fully deintercalated), y = 0.16 (V = 551.37 Å^3 for a fully intercalated and V = 521.66 Å^3 for fully deintercalated) and y = 0.33 (V = 545.34 Å^3 for fully intercalated and V = 521.66 Å^3 a fully deintercalated spinel) was 6.9, 5.3, and 4.22%, respectively, which agreed with results reported in the literature.[12] All Co-substituted phases were more reversible to repeated lithium insertion–deinsertion processes than the pure spinel. The stability of the structure increases with a decrease of the volume shrinkage. However, increasing the cobalt content in the spinel higher than y = 0.16 resulted in a very sharp decrease of capacity. Thus, the optimized Co content in the spinel should not exceed y = 0.16. The improvement of cycle performance was attributed to the stabilization of the octahedral sites in the spinel structure. The binding energies of MnO_2 and CoO_2 are 946 and 1067 kJ/mol, respectively.[12] The stronger CoO_2 bond contributed to the overall stabilization of the spinel octahedral sites.

Figure 4 shows the BET surface area of pure and Co-doped spinels as a function of cobalt content in the oxide. As shown in this figure, substitution of cobalt increases the particle size and decreases the total surface area of the spinel by up to 50%, which is beneficial for good capacity retention properties of the cathode both at room and at high temperatures.[9] After the initial reduction, the spinel surface area remained independent of the Co content in the oxide. Similar results were obtained using SEM. As shown in Fig. 5, a small addition of Co (y = 0.05) resulted in a significant decrease in the surface area and differences in sample morphology between the pure and Co-doped spinel. The Co-doped samples consisted of aggregates of well-developed crystals.

Figure 6a-e shows galvanostatic charge-discharge profiles obtained for $Li_xCo_yMn_{2-y}O_4$ electrodes with y = 0, 0.050, 0.060, 0.160, and 0.330, respectively. For all samples, two distinct plateaus were observed during charging and discharging the electrode which are characteristic of the

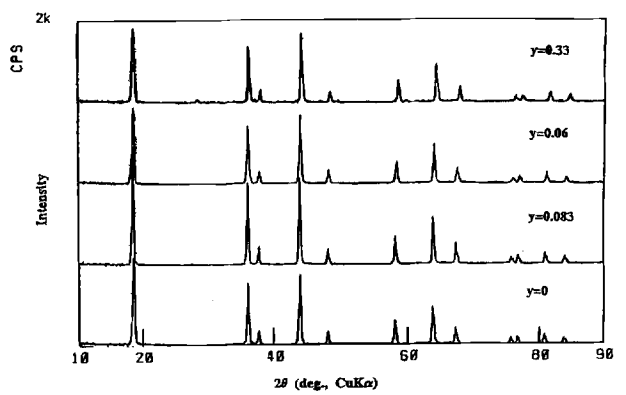

Fig. 2. Powder XRD patterns of $LiCo_yMn_{2-y}O_4$ samples for y = 0, 0.33, 0.16, and 0.083.

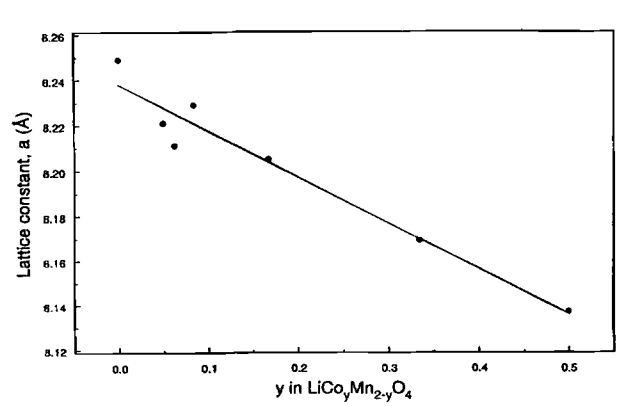

Fig. 3. Lattice constants of $LiCo_yMn_{2-y}O_4$ as a function of Co content in the spinel.

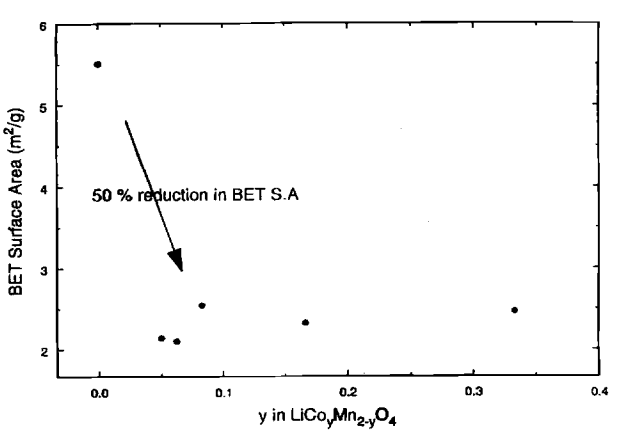

Fig. 4. BET surface areas of pure and Co-doped spinels.

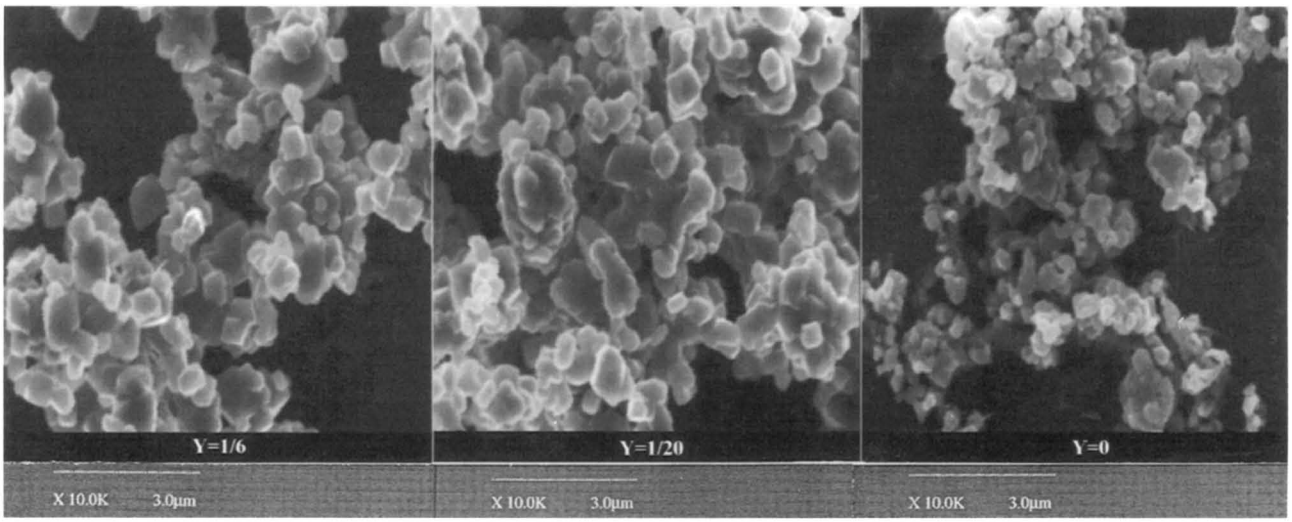

Fig. 5. SEM photographs of $LiCo_yMn_{2-y}O_4$ samples: y = (a) 0, (b) 0.05, and (c) 0.16.

spinel $LiMn_2O_4$ structure. These plateaus correspond to a reversible two-stage process which includes insertion and deinsertion of Li ions in $Li_xCo_yMn_{2-y}O_4$.[1-7] As shown in Fig. 6b and c, both plateaus are easily distinguished in the presence of small amounts of dopant (Co). They tend to merge into one plateau as the concentration of doped Co in $LiMn_2O_4$ increases from y = 0.16–0.33 (Fig. 6d and e). A large capacity loss was observed when cycling the undoped spinel (Fig. 6a) compared to the Co-doped spinel (Fig. 6b-e).

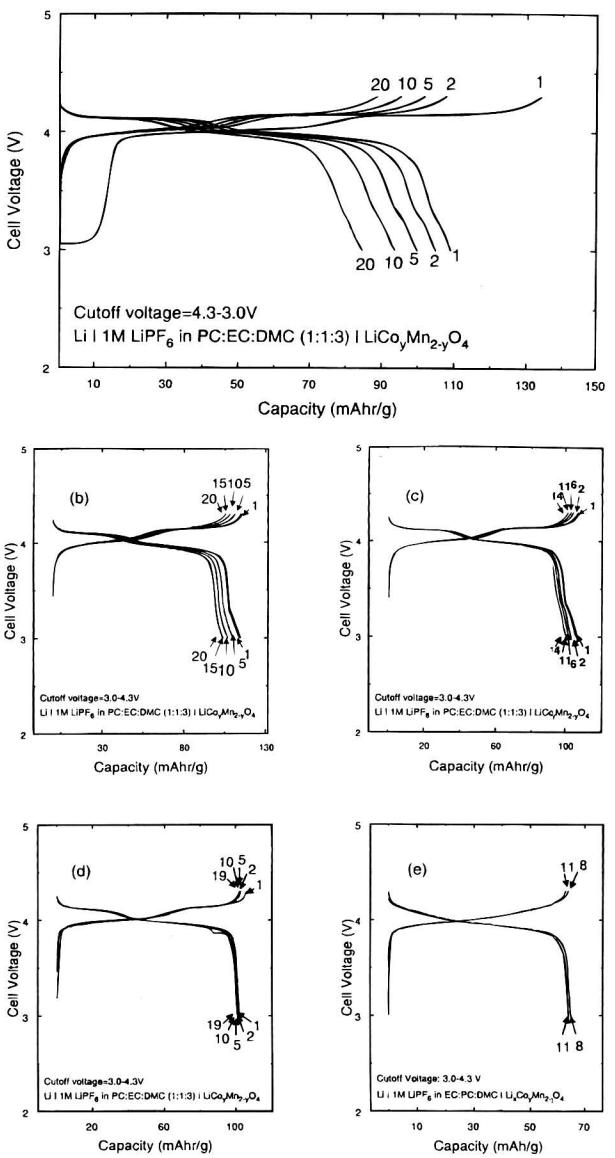

Fig. 6. Galvanostatic charge–discharge curves of (a) pure spinel and (b) $Li/LiCo_yMn_{2-y}O_4$ cells, numbers on the curves represent the cycle number: y = (a) 0, (b) 0.05, (c) 0.06, (d) 0.160, and (e) 0.33.

Figure 7 shows typical galvanostatic cycling curves for the pure and Co-doped spinels. For all Co-doped spinels, the capacity fade decreases substantially with cycle number. Increasing the Co content in the spinel from y = 0 to 0.05 and 0.06 resulted in an increase of the specific capacity and improvement in cycling performance of the cathode active material. With a Co content in the spinel of y = 0.160, a small reduction in the initial capacity was observed. However, as shown in Fig. 7, after the initial decrease in capacity, the y = 0.160 capacity line crosses the capacity decay lines of y = 0.0, 0.060, and 0.050 after 5, 12, and 30 cycles, respectively. Consequently, after 85 cycles, the specific capacity of Co-doped spinel with y = 0.160 is 100 mAh/g compared with specific capacities of 90, 82, and 65 mAh/g for y = 0.050, 0.060, and 0.0, respectively. Similar results were obtained for Co-doped spinels with y = 0.120 and 0.140. Co concentrations higher than y = 0.160 in $Li_xCo_yMn_{2-y}O_4$ resulted in a reduced initial capacity of 70 to 80 mAh/g.

Figure 8 shows the capacities of Co-doped spinels at the 1st and 50th cycles and the capacity loss per cycle as a function of Co content in $LiCo_yMn_{2-y}O_4$ cathode. The capacity loss per cycle was calculated by averaging the capacity loss over the first fifty cycles. The capacity loss

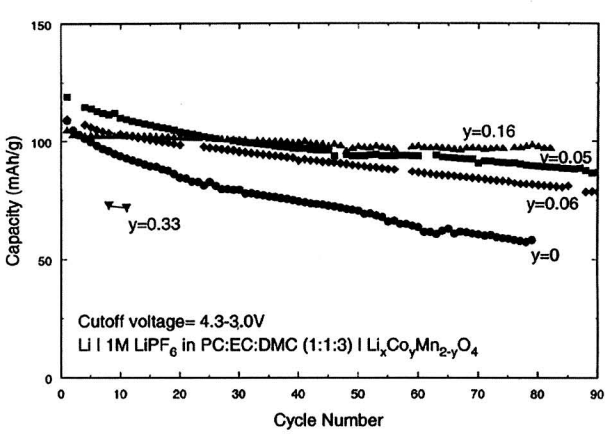

Fig. 7. Variation of the capacity as a function of cycle number for $Li/LiCo_yMn_{2-y}O_4$ cells.

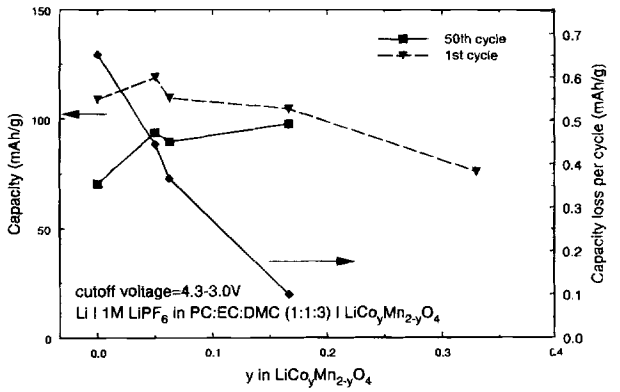

Fig. 8. Capacity and capacity loss per cycle as a function of Co content (y) in $LiCo_yMn_{2-y}O_4$ cells.

per cycle is largest for pure spinel. When increasing the cobalt content in the spinel, the capacity loss of the cathode per cycle reached a minimum when the Co content in the spinel was $y = 0.160$. With a further increase in Co content, the capacity loss per cycle showed a slight decrease. However, a cobalt content in the spinel higher than $y = 0.16$ in $Li_xCo_yMn_{2-y}O_4$ resulted in a reduced initial capacity of 70–80 mAh/g. Thus, an optimized mixed oxide cathode shows an overall capacity of 100–105 mAh/g and a very small capacity fade with y in $Li_xCo_yMn_{2-y}O_4$ in the range 0.160–0.120.

Figure 9 shows the initial cyclic voltammogram obtained for three cathode materials ($y = 0$, 0.160, and 0.33). The experiments were performed using a sweep rate of 0.06 mV/s. The two characteristic peaks of the spinel can be easily distinguished for small amounts of dopant, indicating that a small amount of Co in the spinel does not disturb the host structure. However, the peaks tend to merge into one as the concentration of doped Co in $LiMn_2O_4$ increases to $y = 0.33$. As shown in Fig. 9, increasing the dopant concentration causes the peaks to become smaller and shift toward lower potentials. The observed shift of the peak potential contributes to increased stability of the electrolyte, which results in lower capacity fade of the Co-doped spinel when compared to the pure spinel. As shown in Fig. 9, with a Co content in the spinel of $y = 0.160$, a small reduction of the initial capacity was observed. When the Co content increased to $y = 0.33$ a drastic decrease of the capacity occurred. The capacities of Co-doped spinel with $y = 0.160$ and $y = 0.33$ were 107 and 77 mAh/g, respectively, compared with 110 mAh/g for the pure spinel.

Cyclic voltammograms obtained for samples with $y = 0.06$ and 0.16 in $Li_xCo_yMn_2O_4$ after the 2nd and 85th cycles are shown in Fig. 10a and b. The observed decrease in the peak height and estimated capacity as a function of cycling are in agreement with the observed capacity loss from the galvanostatic charge–discharge profiles presented in Fig. 7. The pure spinel showed a very large capacity fade. From the initial capacity of 107 mAh/g, the capacity decreased up to 65 mAh/g after 65 cycles. The Co-doped spinel with $y = 0.06$ shows a large capacity fade after 85 cycles. From the initial capacity of 109 mAh/g estimated after the 2nd cycle, the capacity decreased to 81 mAh/g after 85 cycles. The Co-doped spinel with $y = 0.160$ in $Li_xCo_yMn_{2-y}O_4$ showed a low capacity fade of only 7 mAh/g in the first 85 cycles.

Determination of electrochemical kinetic parameters for pure and Co-doped spinels using linear polarization and EIS techniques.—The reversible intercalation–deintercalation of Li^+ ions has been studied extensively in layered structures. Since it has been assumed that the diffusion of Li^+ ions within the insertion compound is rate-limiting, the fundamental electrochemical investigations have been limited to studies of Li^+ ionic diffusion. However, the charge-transfer resistance is also an important kinetic parameter, especially in the case of high Li^+ ion mobility within the host.

Linear polarization and EIS techniques were used to determine the total resistance, [charge-transfer resistance (R_{ct}), surface-layer resistance (R_{sl}), and ohmic resistance (R_e)] and exchange current density (i_o) of pure and Co-doped spinels. The experimental procedure was performed as follows: the electrode was charged under constant-current mode to a fully charged state (4.3 V vs Li/Li^+). After the open-circuit potential (OCP) stabilized, linear polarization and EIS experiments were carried out. Then the electrode was discharged for a certain period of time and the same measurements were conducted. The procedure was repeated until the electrode was discharged to the cut-off potential of 3.0 V vs Li/Li^+.

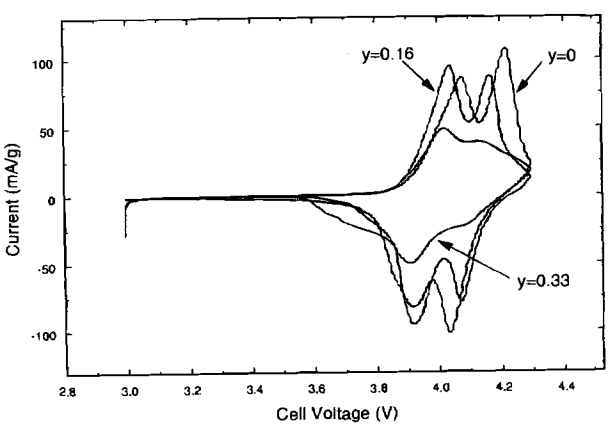

Fig. 9. Cyclic voltammograms of $Li/LiCo_yMn_{2-y}O_4$ cells at a 0.06 mV/s rate.

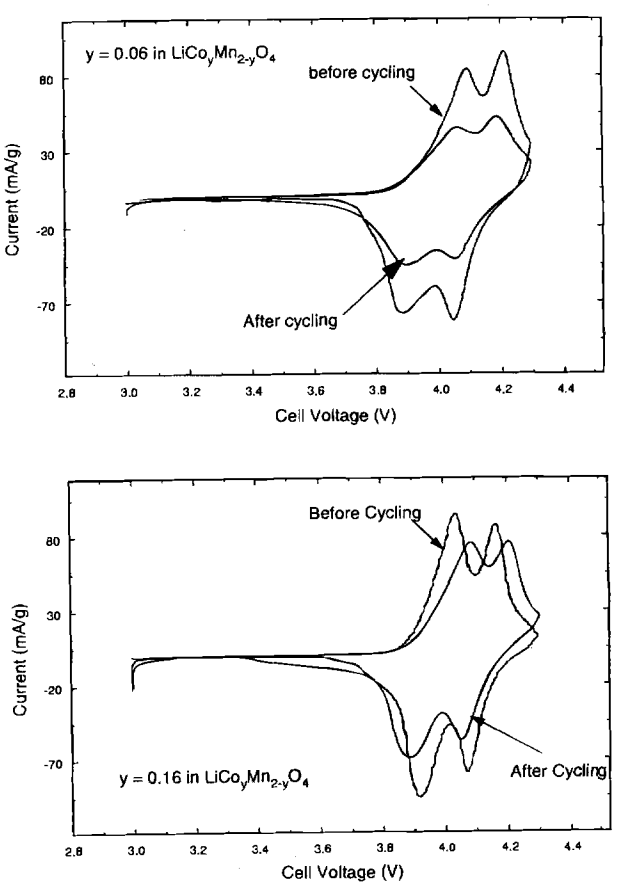

Fig. 10. Cyclic voltammograms obtained for samples with y = (a, top) 0.06 and (b, bottom) in $Li/LiCo_yMn_{2-y}O_4$ after the 2nd and 85th cycles.

The total resistance determined by using the LP technique was equal to the charge-transfer resistance only when the electrode ohmic resistance was negligible.[18,19] In such a case, the charge-transfer current across an interface of active surface area (A) is given by

$$i = AnFk\{a_o \exp[-(1 - \beta)nF\eta/RT] - a_r \exp(\beta nF\eta/RT)\} \quad [1]$$

where k is the charge-transfer rate constant, $n = 1$ for Li^+ ion transfer, and η is the overpotential. The insertion-ion activities in the electrolyte and electrode are represented by a_o and a_r. At low overpotentials, linearization of the Butler–Volmer equation results in

$$R_{ct} = \frac{RT}{Fi_o} = \frac{\eta}{i}; \quad i_o = AnFka_o^{\beta}a_r^{(1-\beta)} \quad [2]$$

where i_o is the exchange current density. However, when the ohmic resistance is not negligible eq 2 estimates a sum of the ohmic resistance and the charge-transfer resistance. Thus, the exchange current density is underestimated. EIS enables a determination of the charge-transfer resistance and an evaluation of the exchange current density without interference of the ohmic resistance.

The Nyquist plots obtained at different states of charge for pure spinel and Co-doped spinels ($y = 0.160$) are shown in Fig. 11a and b, respectively. For both the pure spinel and the Co-doped spinel two semicircles were observed. The semicircle at the low-frequency region represents the charge-transfer resistance and the nonfaradic processes occurring at the electrode–electrolyte interface. Thus, the faradic contribution may be presented as shown in Fig. 11a by a charge-transfer resistance (R_{ct}) and by a Warburg impedance (Z_w) which includes diffusion-controlled processes in the solid. The model assumes that the spinel forms a rough but continuously interconnected, porous solid of low bulk resistance, $R_b < R_e$, where R_e is the electrolyte resistance. At lower frequencies, uniform charging of the electrode surface results in formation of classical double-layer capacitance in the nonfaradic branch of the Nyquist plot. Thus, the nonfaradic contribution in the circuit can be represented by the electrolyte resistance (R_e) and by the double-layer capacitance (C_{dl}).

It is reasonable to assume that the second semicircle is due to the electrolyte decomposition product formed as a result of oxidation-reduction processes occurring on the surface of the electrode. A surface-layer model was used to fit the data. An equivalent circuit for this model is presented in Fig. 11a; R_{sl} represents the insertion-ion resistance and C_{sl} is the capacitance of the surface layer. The data were fitted using Solatron impedance graphing and analysis software ZView (Scribner Associates, Inc).

The charge-transfer resistance values obtained from EIS are compared in Fig. 12 with those estimated using an LP technique. The LP measurements were performed on both pure and Co-doped spinels at different states of charge using a potentiodynamic method at a scan rate of 1 mV/s. As shown in Fig. 12, the charge-transfer resistance values for pure spinel ($y = 0$) were higher than those estimated for Co-doped spinels with an optimized cobalt content of $y = 0.160$. The charge-transfer resistances for both the pure spinel and Co-doped spinel were independent of state of charge (SOC). The average charge-transfer resistance values estimated for pure and Co-doped spinels at different states of charge are 0.27 Ω g (19.9 Ω) and 0.171 Ω g (11.62 Ω), respectively. The presence of Co decreases the charge-transfer resistance and facilitates the charge-transfer reaction in the active material, which is favorable for battery operation.

The exchange current density values were estimated using eq 2 at different states of charge for pure and Co-doped spinel. The charge-transfer resistances used to calculate the exchange current density were estimated by fitting the ac-impedance data and are presented in Fig. 12. The calculated exchange current densities are plotted as a function of the SOC in Fig. 13. The average exchange current densities of the Co-doped spinel ($y = 0.160$) and the pure spinel are 150.63 and 95 mA/g, respectively. The surface area of the pure spinel determined by BET was approximately 5.5 m^2/g, which converts the exchange current density into 1.729×10^{-6} A/cm^2. This value agrees with the exchange current density value of 1.3×10^{-6} A/cm^2 reported in the literature by Kanoh et al.[11] for $LiMn_2O_4$. The surface area of the Co-doped spinel determined by BET was 2.32 m^2/g, which converts the exchange current density into 6.49×10^{-6} A/cm^2.

Figure 14 shows the dependence of C_{dl} values of pure spinel and Co-doped spinel as a function of SOC. The values of C_{dl} estimated for both the pure spinel (average value of 22.5 μF) and Co-doped spinel (average value of 25.32 μF) were independent of the SOC. The results indicated that the effective surface area of the electrode does

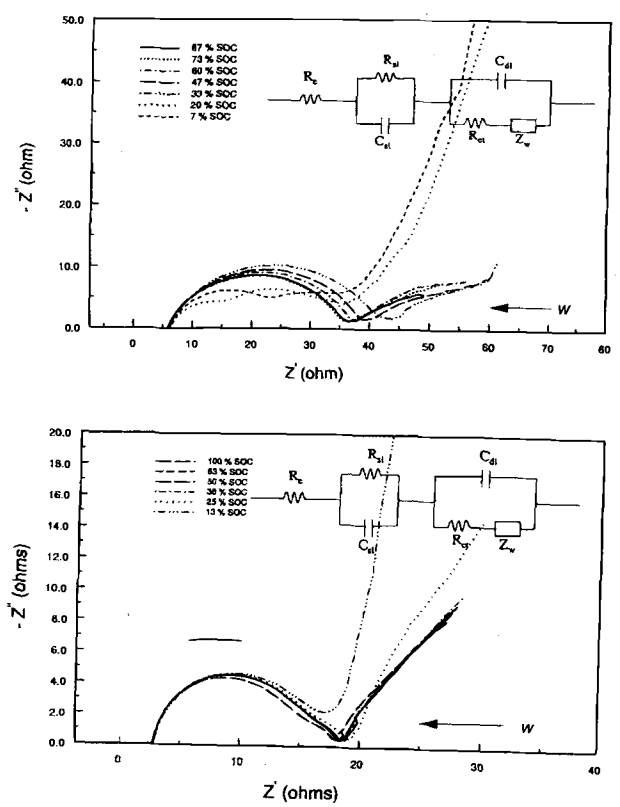

Fig. 11. (a, top) AC impedance spectra of pure spinel obtained at different SOCs, equivalent circuit described in text. (b, bottom) AC impedance spectra of Co-doped spinels obtained at different SOCs, $y = 0.160$ in $Li/LiCo_yMn_{2-y}O_4$.

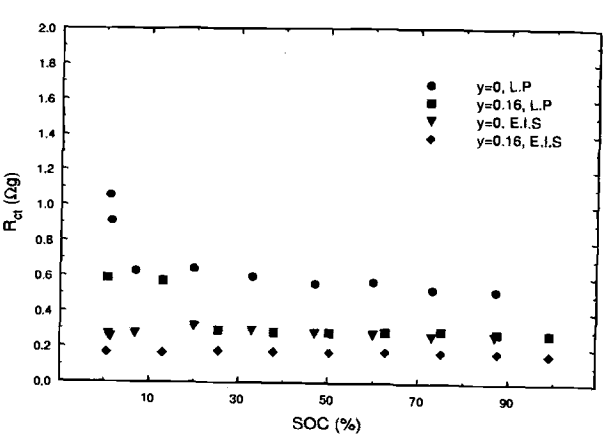

Fig. 12. Charge-transfer resistance (R_{ct}) evaluated from LP and EIS as functions of SOC for $Li/LiCo_yMn_{2-y}O_4$ cells ($y = 0$ and 0.160).

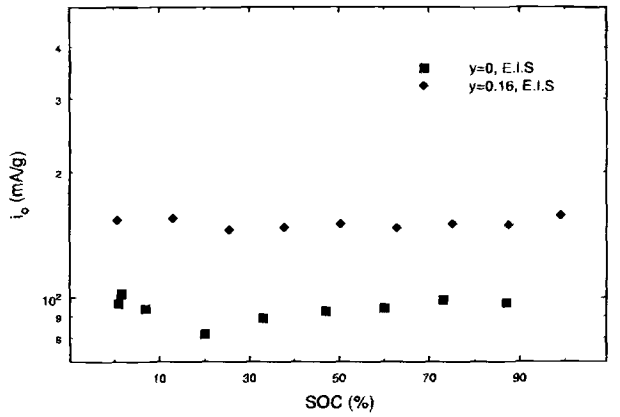

Fig. 13. Exchange current density as a function of SOC for $Li/LiCo_yMn_{2-y}O_4$ cells (y = 0, and 0.160).

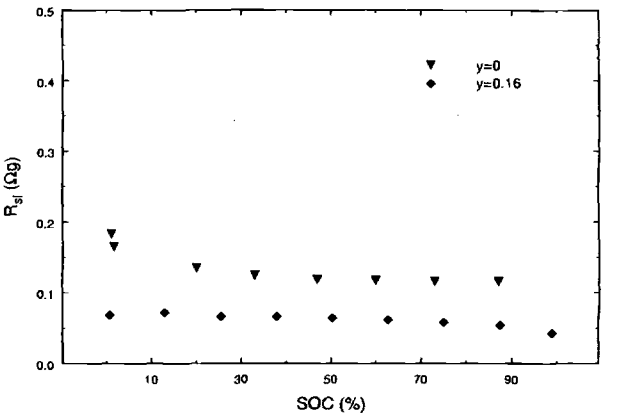

Fig. 15. R_{sl} as a function of SOC for $Li/LiCo_yMn_{2-y}O_4$ cells (y = 0 and 0.160).

not increase significantly with time due to the complete flooding of the electrode with the electrolyte.

Since $R_{sl} = \rho(l/A)$ and $C_{sl} = \epsilon(A/l)$, the surface-layer resistance should increase, while the surface capacitance should decrease with the increase of the surface-layer thickness, l. As shown in Fig. 14, the capacitance of the surface layer is almost independent of the SOC for both the pure and Co-doped spinels, indicating that the thickness of the surface layer formed initially on the surface of the electrode remains constant. Note that the EIS experiments were performed initially on a fully charged electrode. The values of the surface-layer capacitance estimated for the pure spinel at different SOCs were in the range of 3.26–1.9 μF. These values were smaller compared with surface-layer capacitance values estimated for Co-doped spinel (8.16–6.4 μF), indicating that a thicker surface layer formed on the pure spinel. The presence of Co in the spinel inhibits the passivation processes occurring on the surface of the cathode.

According to Fig. 15, the R_{sl} values are independent of SOC for both the pure and Co-doped spinel. The R_{sl} value estimated for the pure spinel increases from 0.11 Ω g (8.7 Ω) for a fully charged electrode to 0.18 Ω g (13.7 Ω) for a fully discharged electrode. The observed increase of resistance is due to slow growth of the film as a function of time. Also, R_{sl} for the Co-doped spinel increased from 0.04 Ω g (2.9 Ω) to 0.07 Ω g (4.7 Ω), in agreement with the estimated decrease of C_{sl} from 3.26 to 1.9 μF and 8.16 to 6.4 μF for pure and Co-doped spinel, respectively. Thomas et al.[20] reported from their impedance analysis of polycrystalline $L_{1-x}CoO_2$ that the rate of growth of the surface layer was rapid over the first 6 h after the construction of the cell and thereafter the films grow slowly.

Determination of Li-ion diffusion coefficient and Li-ion partial conductivity in cobalt-doped spinel.—Under semi-infinite diffusion conditions in the case when the time constants of the different physical processes occurring at the electrode are separated, the Li^+-ion diffusion coefficient can be obtained from an analysis of the Warburg impedance[11,20,21]

$$-\mathrm{Im}Z = B\omega^{-1/2}$$
$$\mathrm{Re}Z = B\omega^{-1/2} \qquad [3]$$

where ω is the angular frequency of the ac perturbation, and B is the Warburg coefficient. The 45° portion of the line in Fig. 11 corresponds to a frequency range where the kinetics of the system are entirely limited by the rate of processes controlled by diffusion. The numerical values can be extracted from eq 4,[11] when $\omega >> D_{Li^+}/L^2$

$$D_{Li^+} = \frac{1}{2}\left[\frac{V_m}{FSB}\frac{dE}{dx}\right]^2 \qquad [4]$$

where F is the Faraday constant, S the apparent geometrical area of the positive electrode, V_m the molar volume of $Li_xCo_yMn_{2-y}O_4$, dE/dx the slope of the OCP vs mobile ion concentration x at each x value, and L is the maximum length of the diffusion pathway. The OCP curves showed a similar loss of resolution of the two plateaus for Co-doped $LiMn_2O_4$ as observed during galvanostatic cycling of these materials (Fig. 6b-e). The Warburg coefficient was obtained from the slope of Re Z vs $\omega^{1/2}$ or −Im vs $\omega^{1/2}$. The D_{Li^+} values as a function of x for both $y = 0$ and $y = 0.160$ in $Li_xCo_yMn_{2-y}O_4$ are presented in Fig. 16. As shown in Fig. 16 for $y = 0$, the D_{Li^+} is in the range 9.20×10^{-14} to 2.6×10^{-12} m^2/s, in agreement with the diffusion coeffi-

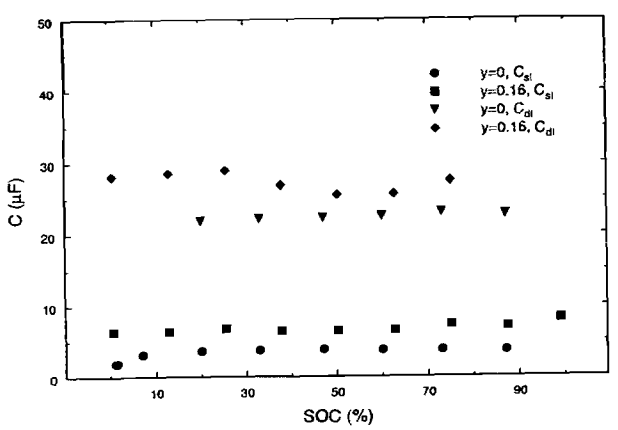

Fig. 14. C_{sl} and C_{dl} as functions of SOC for $Li/LiCo_yMn_{2-y}O_4$ cells (y = 0 and 0.160).

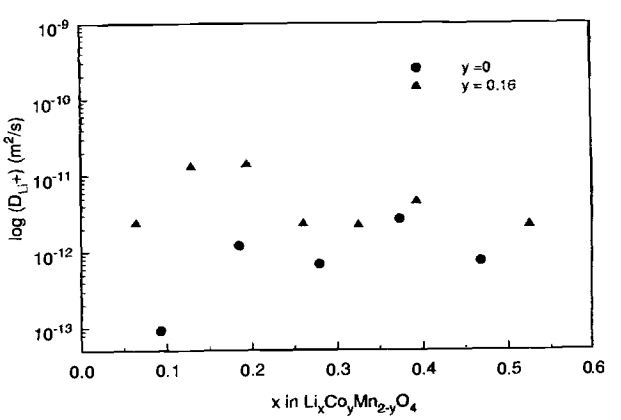

Fig. 16. Chemical diffusion coefficient of Li, D_{Li^+} as a function of x in $Li_xCo_yMn_{2-y}O_4$.

cient reported in the literature.[11] For Co-doped spinel, the diffusion coefficient (D_{Li^+}) was estimated to be in the range 2.4×10^{-12} to 1.4×10^{-11} m^2/s, which is higher then the value estimated for the pure spinel. Guyomard and Tarascon[24] reported a value of 10^{-9} cm^2/s independent of SOC. Recently, Barker et al.[25] reported a range of $(0.2–2.2) \times 10^{-8}$ cm^2/s, with fairly complex dependence on SOC, and Striebel et al.[26] reported a value of 2.5×10^{-11} for $LiMn_2O_4$ thin films measured using the galvanostatic intermittent technique (GITT). The values quoted for the diffusion coefficient are accurate to within an order of magnitude because of the difficulties involved in estimating the true electrochemical area of the cathode material.

The partial conductivity of lithium ion (σ_{Li^+}) was calculated using the equation

$$\sigma_{Li^+} = \left(\frac{FD_{Li^+}}{V_m}\right)\left(\frac{dE}{dx}\right)^{-1} \quad [5]$$

In Fig. 17, the partial conductivity, σLi^+, is presented for $y = 0$ and 0.16 as a function of x in $Li_xCo_yMn_{2-y}O_4$. As shown in this figure, for $y = 0$, the Li^+ partial conductivity varies from (1.2 to 7.2) $\times 10^{-5}$ S/cm. Higher values were estimated for Co-doped spinel ($y = 0.16$) which were in the range between 8×10^{-5} and 1.85×10^{-4} S/cm. The observed low σ_{Li^+} value indicates a predominant contribution of electronic conductivity to the total conductivity in the spinel.

Self-discharge studies.—Self-discharge up to 6–12% in the first month occurs in oxidized $LiMn_2O_4$, $LiCoO_2$, and $LiNiO_2$ electrodes.[9,10] The capacity loss depends upon factors such as the cathode and cell preparation, the nature and purity of the electrolyte, temperature, and the storage time. Self-discharge losses can be both reversible and irreversible. The reversible capacity loss is recovered by charging the cell while the irreversible capacity loss is not recoverable and contributes to the overall capacity fade of the cell. The self-discharge processes are caused in the charged state of the electrode by the highly oxidizing and reducing character of the electrode materials and the electrolyte, respectively.[9]

Figure 18 shows the initial voltage decay for pure and Co-doped fully charged spinels upon storage in 1 M $LiPF_6$-PC:EC:DMC (1:1:3) electrolyte. The self-discharge rate in the case of the pure spinel is 41.5 mV/day compared with 31.2 mV/day for Co-doped ($y = 0.160$) spinels. Thus, Co stabilizes the spinel structure while reducing the self-discharge rate. The lower self-discharge rate of Co-doped spinels can be also attributed to their low surface areas (Fig. 4 and 5) compared with the high surface area of pure spinels. The larger particle size of Co-doped spinels results in lesser contact between the active material and the electrolyte, thus decreasing the rate of both the electrode and the electrolyte decomposition.

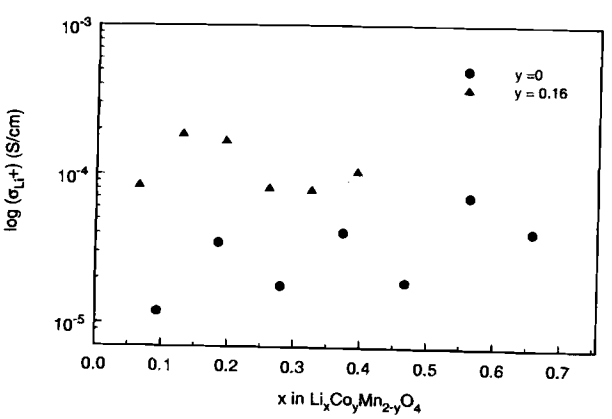

Fig. 17. σ_{Li} as a function of x in $Li_xCo_yMn_{2-y}O_4$.

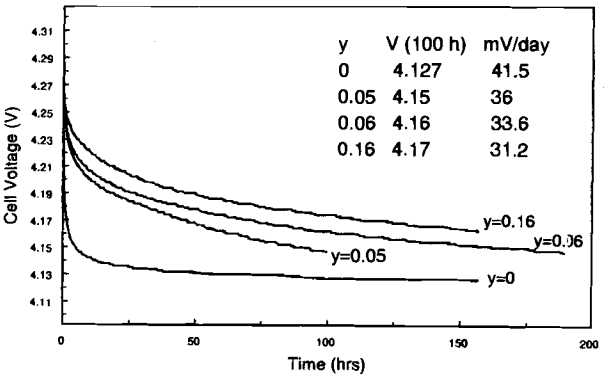

Fig. 18. The cathode voltage decay as a function of storage time in 1 M $LiPF_6$-PC:EC:DMC (1:1:3).

Potentiostatic experiments were also carried out to determine the nature of the discharge process occurring at the cathode. The cathode was oxidized up to 4.3 V and the potential was kept constant during the experiment. Under these conditions, one measures the floating current, that is, the current required to counterbalance the self-discharge. The floating current and the capacity loss for a pure spinel are shown in Fig. 19a, and in Fig. 19b-d for Co-doped spinels. The cumulative capacity losses for pure and Co-doped spinels are compared in Fig. 20. The capacity loss estimated for pure spinel resulting from self-discharge in the first 30 h is 3 and 6 times larger than those for Co-doped spinel with $y = 0.06$ and 0.160, respectively. These results are in agreement with the voltage decay curves presented in Fig. 18.

The effect of storage on the cycling ability of Co-doped spinels was also investigated. Figure 21 shows the results obtained for an oxidized Co-doped spinel ($y = 0.16$) before and after storage for 150 h. The cell cycled after 150 h of storage showed a larger capacity fade with increasing number of cycles, compared to a cell which was cycled fresh. This capacity loss can be attributed to passive-film formation resulting from the electrolyte-decomposition products.

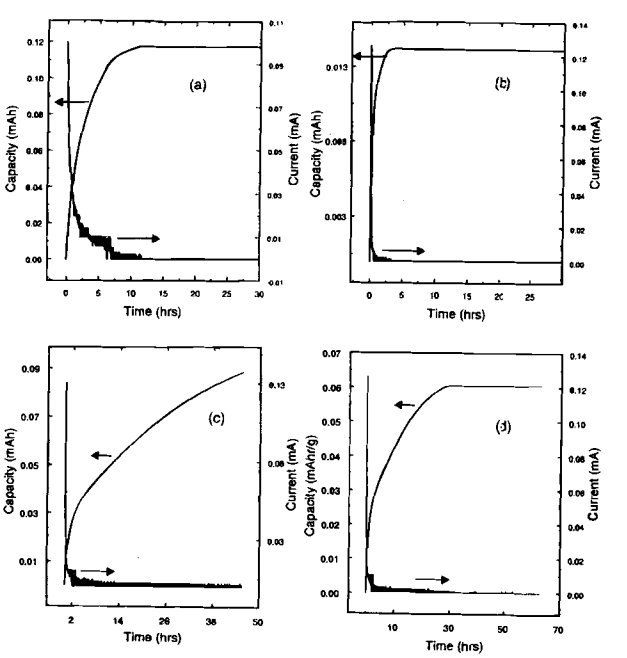

Fig. 19. Cumulative capacity (left ordinate) and floating current (right ordinate) for Li/$LiCo_yMn_{2-y}O_4$ cells with y = (a) 0, (b) 0.160, (c) 0.06, and (d) 0.050.

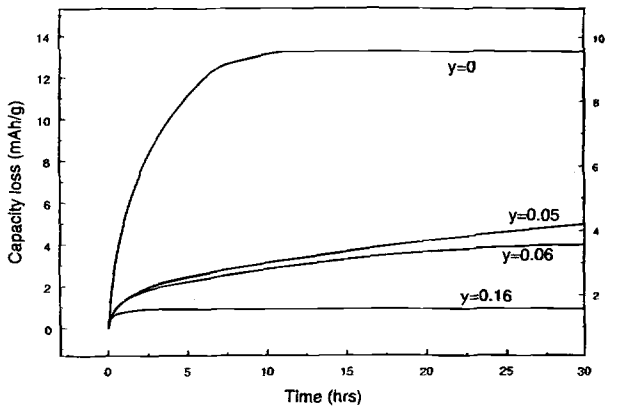

Fig. 20. Cumulative capacity loss during self-discharge for Li/LiCo$_y$Mn$_{2-y}$O$_4$ cells with y = 0, 0.160, 0.06, and 0.050.

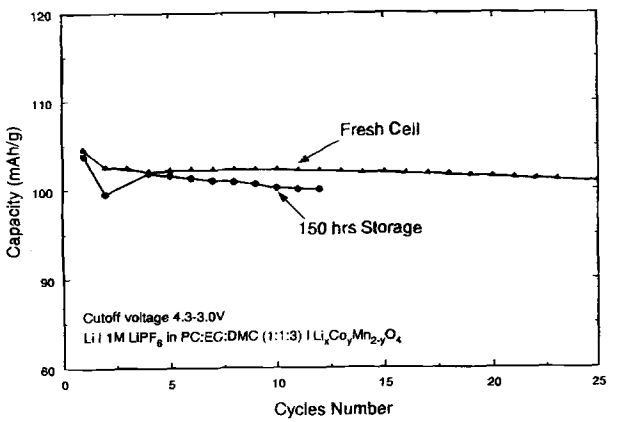

Fig. 21. Cycling behavior of a Li/LiCo$_y$Mn$_{2-y}$O$_4$ cell with y = 0.160 with (150 h storage) and without previously aged electrodes.

Conclusions

Substitution of Co in $Li_xMn_2O_4$ increases the particle size and decreases the total surface area of the spinel by up to 50%, which is beneficial for good capacity retention properties of the cathode. After the initial reduction of the surface area observed for y = 0.05 in $LiCo_yMn_{2-y}O_4$, the spinel surface area remained independent of the Co content in the oxide. Increasing the Co content in the spinel from y = 0 to y = 0.05 and 0.06 resulted in an increase in initial capacity and a decrease in capacity fade during cycling. With a Co content in the spinel of y = 0.160, a small reduction in the initial capacity was observed. However, after the initial decrease in capacity, the y = 0.160 sample capacity curve crossed the capacity decay curves of y = 0.0, 0.060, and 0.050 after 5, 12, and 30 cycles, respectively. The specific capacity of a Co-doped spinel with y = 0.160 is 100 mAh/g compared with specific capacities of 90, 82, and 65 mAh/g estimated for y = 0.050, 0.060, and 0.0, respectively. Similar results were obtained for Co-doped spinels with y = 0.120 and 0.140.

The charge-transfer resistance for the pure and Co-doped spinels were 0.27 Ω g (19.9 Ω) and 0.171 Ω g (11.62 Ω), respectively. The charge-transfer resistance values for both the pure and Co-doped spinels were independent of SOC. The average exchange current densities estimated for Co-doped spinel (y = 0.160) and pure spinel are 6.59 × 10^{-6} and 1.73 × 10^{-6} A/cm^2. The presence of Co increases the charge-transfer resistance and facilitates the charge-transfer reaction in the active material, which is favorable for battery operation.

The surface resistance values, (R_{sl}) were independent of SOC and varied from 0.11 Ω g (8.7 Ω) for a fully charged electrode to 0.18 Ω g (13.7 Ω) for a fully discharged electrode. The observed increase of the resistance was due to the slow growth of a passive film on the surface of the cathode as a function of time. The observed increase of R_{sl} values is in agreement with the estimated decreases of C_{sl} from 3.26 to 1.9 μF and 8.16 to 6.4 μF for pure and Co-doped spinels, respectively. The lithium-ion diffusion coefficient (D_{Li^+}) for Co-doped spinel was estimated to be in the range 2.4 × 10^{-12} to 1.4 × 10^{-11} m^2/s as a function of SOC and was found to be higher than the value estimated for the pure spinel (9.20 × 10^{-14} to 2.6 × 10^{-12} m^2/s). The Li^+ partial conductivities estimated in Co-doped spinel (in the range between 8 × 10^{-5} and 1.85 × 10^{-4} S/cm) were higher than those estimated for pure spinels [(1.2–7.2) × 10^{-5} S/cm].

The larger particle size of Co-doped spinel resulted in less contact between the active material and the electrolyte, contributing to decrease of the rate of electrolyte and electrode decomposition, and consequently, to a smaller self-discharge rate.

Acknowledgments

The authors gratefully acknowledge the financial support provided by DOE Division of Chemical Sciences, Office of Basic Energy Sciences, G.M. DE-FG02-96ER 146598, and by the Office of Research and Development, CIA, under Contract No. 93-FI48100-100.

Manuscript submitted August 6, 1997; revised manuscript received October 10, 1997.

The University of South Carolina assisted in meeting the publication costs of this article.

LIST OF SYMBOLS

a_o	insertion ion activity of oxidized species
a_r	insertion ion activity of reduced species
A	effective surface area, m^2/g
B	Warburg coefficient, Ω s$^{1/2}$
C_{dl}	double-layer capacitance, μF
C_{sl}	surface-layer capacitance, μF
D_{Li^+}	diffusion coefficient of Li ion in positive electrode, m^2/s
E	open-circuit potential, V
F	Faraday's constant, 96,487 C/equiv
i	current per unit of mass, A/g
i_o	exchange current per unit of mass, A/g
Im	imaginary
k	rate constant
l	surface-layer thickness, m
n	number of electrons
R	gas constant, 8.314 J/(mol K)
Re	real
R_b	bulk resistance, Ω
R_e	electrolyte resistance, Ω
R_{ct}	charge-transfer resistance, Ω g
R_{sl}	surface-layer resistance, Ω g
S	apparent geometric area, m^2
t	time, s
T	temperature, K
u	oxygen positional parameter
V	unit cell volume, cm^3
V_m	molar volume, cm^3/mol
x	stoichiometric coefficient for positive electrode, $Li_xCo_yMn_{2-y}O_4$
y	dopant (Co) concentration
Z	impedance, Ω
Z_w	Warburg impedance, Ω

Greek

β	symmetry factor, dimensionless
ϵ	permittivity
σ	conductivity, S/cm
ω	angular frequency, Hz
η	overpotential, V
ρ	resistivity

REFERENCES

1. K. M. Abraham, *J. Power Sources*, **7**, 43 (1981).
2. K. Ozawa, *Solid State Ionics*, **69**, 212 (1994).
3. J. M. Tarascon, E. Wang, F. K. Shokoohi, W. R. McKinnon, and S. Colson, *This Journal*, **138**, 2859 (1991).
4. G. Pistoia, G. Wang, and C. Wang, *Solid State Ionics*, **58**, 285 (1992).

5. R. J. Gummow, A. DeKock, and M. M. Thackeray, *ibid.*, **69,** 59 (1994).
6. I. J. Davidson, R. S. McMillan, and J. J. Murray, *J. Power Sources,* **54,** 205 (1995).
7. C. Sigala, D. Guyomard, A. Verbaere, Y. Piffard, and M. Tournoux, *Solid State Ionics,* **81,** 167 (1995).
8. T. Ohzuku, M. Kitagawa, and T. Hirai, *This Journal,* **137,** 769 (1990).
9. D. Guyomard and J. M. Tarascon, *ibid.,* **140,** 3071 (1993).
10. G. Pistoia, A. Antonini, R. Rosatti, and D. Zane, *Electrochim. Acta,* **41,** 2683 (1996).
11. H. Kanoh, Q. Feng, T. Hirotsu, and K. Ooi, *This Journal,* **143,** 2610 (1996).
12. L. Guohua, H. Ikuta, T. Uchida, and M. Wakihara, *ibid.,* **143,** 178 (1996).
13. V. Manev, B. Banov, A. Momchiler, and A. Nassalevska, *J. Power Sources,* **57,** 99 (1995).
14. G. Pistoia, D. Zane, and Y. Zhang, *This Journal,* **142,** 2551 (1995).
15. W. Baochen, X. Yongyao, F. Li, and Z. Dongjiang, *J. Power Sources,* **43-44,** 539 (1993).
16. L. Sanchez and J. L. Tirado, *This Journal,* **144,** 1939 (1997).
17. G. Li, H. Ikuta, T. Uchida, and M. Wakihara, *ibid.,* **143,** 178 (1996).
18. G. Zheng, B. N. Popov, and R. E. White, *ibid.,* **143,** 435 (1996).
19. G. Zheng, B. N. Popov, and R. E. White, *ibid.,* **143,** 834 (1996).
20. M. G. S. R. Thomas, P. G. Bruce, and J. B. Goodenough, *This Journal,* **132,** 1522 (1985).
21. C. Ho, I. D. Raistrick, and R. A. Huggins, *ibid.,* **127,** 343 (1980).
22. D. Guyomard and J. M. Tarascon, *Solid State Ionics,* **69,** 222 (1994).
23. G. Barral, J. P. Diard, and C. Motella, *Electrochim. Acta,* **29,** 239 (1984).
24. D. Guyomard and J. M. Tarascon, *This Journal,* **139,** 937 (1992).
25. J. Barker, R. Pynenburg, and R. Koksbang, *J. Power Sources,* **52,** 185 (1994).
26. K. A. Striebel, C. Z. Deng, S. J. Wen, and E. J. Cairns, *This Journal,* **143,** 1821 (1996).

Oxygen Reduction Characteristics of Heat-Treated Catalysts Based on Cobalt-Porphyrin Ion Complexes

Tatsuhiro Okada

National Institute of Materials and Chemical Research, MITI, Higashi 1-1, Tsukuba, Ibaraki 305, Japan

Masanori Gokita,[a] Makoto Yuasa,[a,b] and Isao Sekine*[,a,b]

[a]*Department of Industrial Chemistry, Faculty of Science and Technology, Science University of Tokyo, 2641 Yamazaki, Noda, Chiba 278, Japan*
[b]*Institute of Colloid and Interface Science, Science University of Tokyo, 1-3 Kagurazaka, Shinjuku, Tokyo 162, Japan*

ABSTRACT

Oxygen reduction characteristics of graphite electrodes modified with aggregated cobalt-porphyrins heat-treated at various temperatures and then impregnated in Nafion polymer were investigated systematically The aggregated cobalt-porphyrin compound was adsorbed on graphite powder and then heat-treated at various temperatures ranging from 200 through 1200 °C. The catalysts were evaluated for electroreduction performances of oxygen on modified electrodes in sulfuric acid solutions. The electrocatalytic performances of catalysts as measured in rotating ring-disk electrodes showed that the most effective catalytic activity for oxygen reduction was attained for the aggregated cobalt-porphyrin compounds on graphite powder heat-treated at temperatures between 600 and 800 °C. The surface concentration of Co and N as measured by X-ray photoelectron spectroscopy increased as the heat-treatment temperature was increased up to 800 °C. The electrochemical performance of pyrolyzed cobalt-porphyrin catalysts changed in parallel with the surface concentration of Co and N. In the temperature range 600-800 °C, it appeared that the increased catalytic activity originated from the well-dispersed Co-N_4 moiety or from fragments of the original molecules still retaining the cobalt bound to nitrogen atoms. In the higher temperature region, Co-N_4 bonds were no longer detected, and the presence of cobalt in the metallic states (β-Co) in the catalysts was confirmed by X-ray diffraction analysis. From the results of the stability tests, the pyrolyzed cobalt porphyrin electrode systems were found to be more stable than the nonheat-treated catalysts.

Introduction

Polymer electrolyte fuel cells (PEFCs) are particularly attractive for transportation and other small scale on-site power source applications because of their high power density at low temperature operations. In the cathodes of PEFCs, platinum supported on carbon is usually used as the catalyst for electroreduction of oxygen. Since Pt is an expensive metal with a relatively limited abundance, various kinds of non-Pt catalysts have been explored.

The metalloporphyrins, phthalocyanines, and related compounds have been extensively investigated in detail as possible catalysts for oxygen reduction.[1-5] Although metalloporphyrin compounds show some catalytic ability, heat-treated porphyrin compounds adsorbed on carbon have been revealed to exhibit higher activity and stability as compared with nonheat-treated ones.

Yeager et al. reported that during the heat-treatment of carbon supported metalloporphyrins at temperatures above 700 °C, macrocycles are pyrolyzed to yield a carbonaceous layer with substantial surface nitrogen as the adsorption sites.[6] The metal may also be present on the surface in the form of small oxide particles, which are to some extent stabilized on this type of surfaces in acid electrolytes. On the other hand, van Veen et al. have explained that metal-N_4 moiety of the chelate is the structural feature associated with the high activity of the heat-treated macrocycles on the surface of carbon materials.[7] However, different views about this activity and stability have been reported by other workers and this point is still not resolved.

In the previous work, it has been shown that the cobalt-porphyrin ion complexes, which are electrostatic aggregates of cobalt tetrakis(4-carboxyphenyl) porphyrin (CoTCPP, anionic) and cobalt tetrakis(1-methyl-4-pyridyl) porphyrin (CoTMPyP, cationic) have a catalytic activity for the reduction of molecular oxygen in acidic solutions.[8,9]

* Electrochemical Society Active Member.
[a] Present address: Toyo Engineering Company, Limited, Kokura, Chiba 264, Japan.